Brokering Spectrum Sharing using Dynamic Spatial-Spectral Masks

Adam C. Goad, *Graduate Student Member, IEEE*, Sarah A. Seguin, *Senior Member, IEEE*, Charles Baylis, *Senior Member, IEEE*, Trevor Van Hoosier, *Graduate Student Member, IEEE*, Emma Lever, *Graduate Student Member, IEEE*, Albin J. Gasiewski, *Fellow, IEEE*, Aravind Venkitasubramony, *Graduate Student Member, IEEE*, and Robert J. Marks II, *Life Fellow, IEEE*

Abstract—Continued spectral crowding can potentially affect the operation of critical passive devices, such as radiometers and radio telescopes. Proliferation of Fifth-Generation (5G) wireless communication systems in the 24 – 30 GHz band could cause massive interference with satellite-based radiometers that operate in the 23.6 – 24.0 GHz (from out-of-band spurious emissions) and the 50 – 58 GHz bands (from spurious harmonic operation of 5G systems). A brokering system is presented to protect crucial passive devices from unwanted interference by coordinating with active systems and limiting both in-band and out-of-band electromagnetic emissions from the active systems. Based on interference criteria presented by the passive systems to the broker, a spatial-spectral mask is created to limit the transmission of the active device in both the spatial and frequency domains.

Index Terms—Spectrum sharing, radiometers, fifth generation (5G), frequency assignment, spurious emissions, electromagnetic interference

I. INTRODUCTION

The electromagnetic spectrum is becoming an increasingly precious resource due to the demands of existing critical devices and new technologies. Traditional static allocations of spectrum, allowing for unencumbered device operation, are rapidly becoming a bygone concept. Importantly, passive spectrum users, such as weather radiometers, are impacted by even very low levels of electromagnetic interference, requiring more complex solutions to address their unique spectrum needs. Fifth-Generation (5G) wireless communication systems have been allocated bands between 24 – 40 GHz, and specifically the designated subbands as listed in Table I.

Subband	Frequency Designation	Common
Designation	Range (GHz)	Reference
n258	24.25 to 27.50 GHz	"26 GHz"
n261	27.50 to 28.35 GHz	"28 GHz"
n257	26.50 to 29.50 GHz	"28 GHz"
n260	37 to 40 GHz	"39 GHz"

Unfortunately, 24 – 30 GHz 5G devices may undesirably interfere with satellite- and ground-based water-sensing radiometers operating in the 23.6 – 24.0 GHz band due

This work has been funded by the National Science Foundation (Grant No. 2030243)

Manuscript received xxx; revised xxx

to adjacent-band intermodulation products. Second, oxygensensing radiometers operating in the 50 - 58 GHz band can be affected by second-harmonic distortion products from the 24 – 30 GHz 5G transmitters. Even slight interference from these 5G systems could impair these vulnerable radiometers, reducing sensitivity and resulting in missed or incorrect weather predictions. Lubar indicates that there could be delays of up to 3 to 6 hours in the accuracy of a three-day forecast, possibly placing thousands of people at risk during a weather disaster, and emphasizes that international regulators must provide protection to weather radiometers from other users [1]. In addition, the former Acting Chief Niel Jacobs of the National Oceanic and Atmospheric Administration (NOAA) expressed concern that there could be a 30 percent reduction in weather forecast accuracy due to possible interference from 5G transmitters, postulating that weather predictions could be reduced to the accuracy levels available in the 1980s as a result of this interference [2]. Rapid climate change and severe weather events such as hurricanes, tornados, and other extreme weather events require precise knowledge of weather for safety and preparedness reasons. The U.S. House of Representatives Committee on Science, Space, and Technology describes the critical nature of weather sensing infrastructure and radiometers and insists on 5G infrastructure improvements [3].

Specific surveys on spectrum sharing have examined extensively how active transmitting devices can share between themselves [4]. In addition, other works have further examined spectrum sharing and allocation for cognitive radio networks and the Internet of Things, waveform flexibility for network slicing, and the specifics of sharing for 5G systems [5]-[7]. However, a comprehensive sharing mechanism between active transmitting devices and passive devices, which do not transmit, is lacking. Passive radiometers and radio astronomy sensors are especially vulnerable to interference, including out-of-band interference from intentional transmitters, and require more complex coordinating solutions such as brokering schemes [8], [9]. Höyhtyä presents controlled spectrum sharing of satellite systems using a database [10], and Luo specifically discusses satellite sharing using a geo-location database [11]. Zulfigar presents policy-specific brokers designed to allocate spectrum solely by market demands [12]. Generally, passive devices would be neglected in all of these specific scenarios, focusing only on the market value of spectrum for

Two prominent examples of spectrum sharing systems are

the Spectrum Access System (SAS) and Automated Frequency Coordination (AFC). The SAS is a cloud-based spectrum manager with a three-tier hierarchical system that manages wireless communications in the 3.5 GHz CBRS band from 3.55 – 3.70 GHz. SAS uses Environmental Sensing Capability (ESC) sensors along with a database of registered transmitter information to manage spectrum allocation. Their main goal is to prevent radio interference (coming from lower-tier members) from affecting their highest priority members or incumbents. These highest priority devices are active devices that belong to the military and government organizations such as radar [13].

The AFC is a spectrum use coordination system that consists of a registered database of information on radio frequency services in a particular area for the 6 GHz band (5.925 7.125 GHz). The priority is given to already existent 6 GHz users, such as fixed satellite services (FSS), used in the broadcast of essential services that already have a license for 6 GHz [14]. This system will coordinate the already existing incumbent users with new unlicensed users of Wi-Fi 6E and other future systems [15].

Spectrum sharing has also been extensively examined in the scenario of cognitive radar systems that can avoid interference from wireless communication transmissions [16]–[19]. These cognitive radar systems all contain feedback, the capability to perform waveform adaptation, and associated signal processing [17]–[19]. These radar systems sense the spectrum and frequencies of interference, then modify their electromagnetic transmissions to coexist with other radiating devices in the electromagnetic spectrum [17]–[22]. Spectral prediction with cognitive radars has also been used to determine possible interferers in the spectrum to further the decision making process [23]. The critical need for spectrum sharing and the understanding of interference has also been examined for automotive radars [24], [25].

In response to knowledge of the communicated spatialspectral mask limitations, systems can often adapt and reconfigure to avoid interference. For example, reconfigurable impedance tuning of array power amplifiers can be used to maximize system performance while minimizing unwanted out-of-band and out-of-beam interference caused by device nonlinearities. It has been shown that the radars transmitter power amplifier (PA) output power depends on the load impedance provided to the active device and the radars bandwidth, transmit frequency, and waveform [26], [27]. In addition, tuning architectures that implement impedance tuning can be performed on the transmitter power amplifier in real time, providing the potential for higher gain when compared to a fixed, broadband matching network, maximizing radar device operation and the ability to adaptively share the spectrum [28], [29]. These solutions all focus on adapting to multiple active transmitting devices and their use of the spectrum.

This paper presents a brokering system with a simple method that addresses and adapts to the specific needs of passive device users. Specifically, this work is focused on coexistence between $23.6-24.0~\mathrm{GHz}$ and $50-58~\mathrm{GHz}$ radiometers and 5G transmitter arrays in the $24-30~\mathrm{GHz}$ band, but presents an approach that is applicable to coexistence

between active and passive spectrum-use systems in other bands and applications. In contrast to SAS and AFC systems which typically provide updates on a daily basis, this broker is designed to communicate with users on timescales measured in seconds or minutes, allowing for even more opportunities for spectral sharing. Key factors that impact scalability include the computational capabilities of the broker and the potential for aggregate interference in a situation where many devices are present. Through a multi-level culling process, the broker is designed to minimize computation time by considering first the simplest computations to determine overlap at the earliest stages of the culling process, eliminating as many pairs with as few computations as possible [9]. While aggregate interference could cause the prediction of harmful interference to be incorrect in cases where multiple devices provide interference in the same band, the assessment of this issue is saved for future work.

2

II. SPATIAL-SPECTRAL BROKER APPROACH

The cooperative brokering system for passive and active devices considers both in-band and out-of-band emissions. The brokering system can calculate a spatial-spectral mask for use by a 5G transmitter aperture to avoid interference with radiometers and other critical passive systems. Fig. 1 illustrates a simple diagram of possible interactions between a passive radiometer and an active 5G communications system. Both active and passive devices send requests to operate within a certain spectrum allocation to the broker. Fig. 2 shows a block diagram representing the optimization process of the broker. Multiple radiometers and 5G systems send transmission requests simultaneously to the broker, and the broker determines the spectral and spatial operation allowances for each radiometer and 5G transmitter. It then communicates these allowances to all users. Based on these spectral and spatial operation allowances, the 5G transmitter controller then has the opportunity to optimize its beam pattern and the reconfigurable power-amplifier (PA) matching networks. This allows maximization of 5G transmitter range and power efficiency within the specified constraints given by the broker.

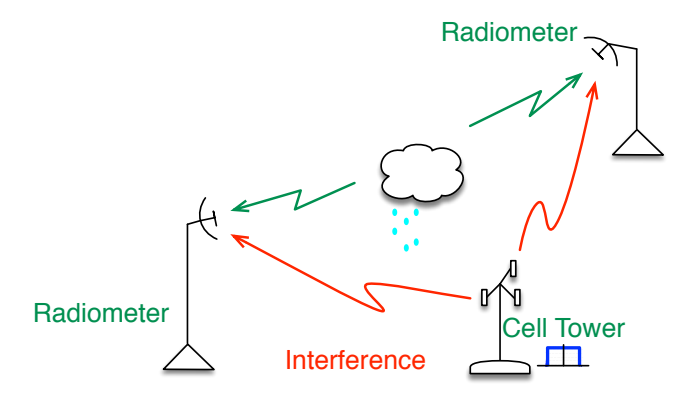


Fig. 1. Passive (radiometer) and active device interaction.

Table II shows the parameters included in each request, with the set of parameters that are labeled as a "manifold"

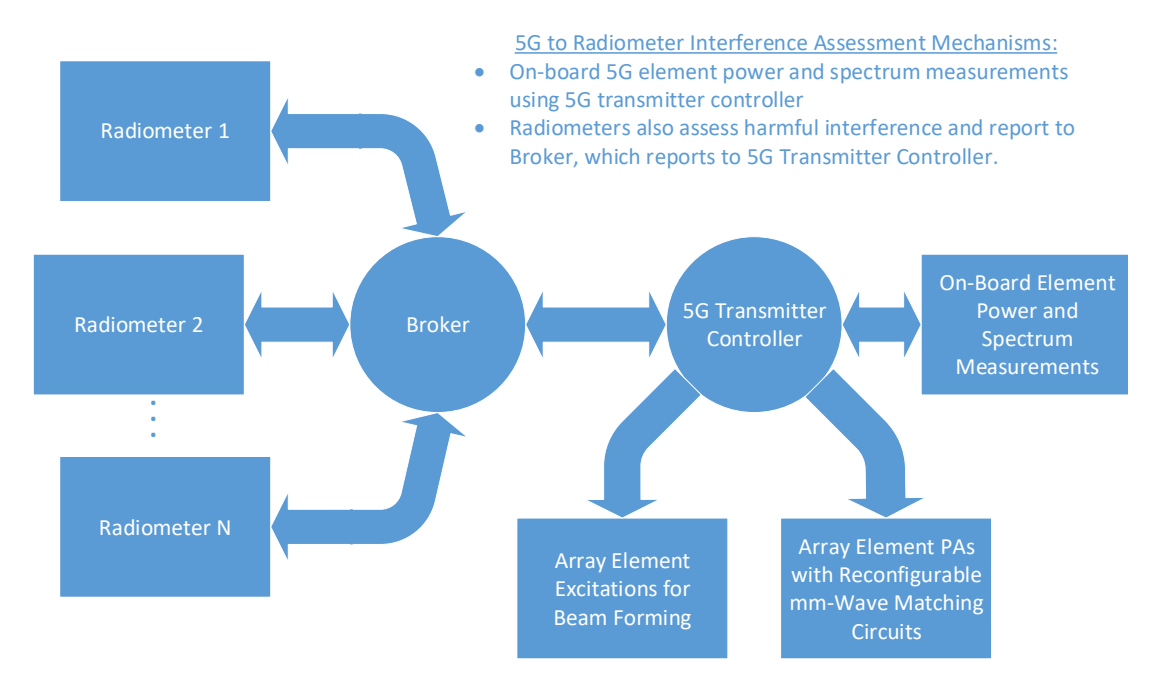


Fig. 2. Block diagram describing the collaboration between radiometers and a 5G Artificially Intelligent Power Amplifier Array (AIPAA) transmitters using a broker-based system for coordination.

[9]. Each device provides its desired spectral, spatial, and temporal occupancy, as well as other specifics such as transmit power and receiver interference power tolerance. Based on the information from each device, the broker assesses the potential for interference between each pair of devices using a scalable culling process. The broker returns a "go" or "no go" flag, describing whether a direct overlap of space, time, and frequency parameters has been observed. Even in a "go" situation, out-of-band or harmonic interference may be possible. If this is the case, out-of-band and harmonic emission constraints are communicated to the potentially interfering transmitter. The constraints are provided in the form of a dynamically adaptive spatial-spectral mask.

TABLE II REQUIRED INFORMATION FOR A COLLABORATIVE BROKER

Data Requested	Units	Symbols
Start Time	seconds	t
Time Duration	seconds	Δt
Latitude	decimal degrees	φ
Longitude	decimal degrees	λ
Altitude	meters	a
Center Frequency	hertz	f
Bandwidth	hertz	BW
Azimuth	degrees	α
Elevation	degrees	β
Beamwidth	degrees	θ
Transmitter Power	dBm	P_{Tx}
Receiver Power Tolerance	dBm	T
Antenna Gain	dBi	$G_{Tx/Rx}$

Fig 3 depicts a flow diagram for how the broker is designed to control interference between given devices based on their request manifolds. For each pair of requests, at each level of the culling process, comparison between the requests is performed for one parameter set at a time to see if an

overlap, resulting in potential interference, is obtained. There are five stages of culling: (1) Time Overlap, (2) Frequency Interference Calculation, (3) Friis Tolerance, (4) Line of Sight, and (5) Cone Intersection. Each stage compares all device manifolds. If the determined interference-free condition is met for a specific stage, the comparisons of the device manifolds continue to the next stage until completing the entire process. The stages are designed so that, if at any stage an interference criterion is not met (for example, devices will not operate at the same time), then it is determined that these devices cannot interfere and the broker exits the culling process, indicating that the pair of devices in question does not present a potential interference situation. The order of culling presented here is completed in the most computationally efficient manner, completing the least complex calculation and moving to the next complex so that the broker may efficiently and quickly address each culling stage. However, if overlap is seen for each of the five culling levels, the broker then provides a "no-go" to the active device if the comparison is between active and passive systems, or provides a "no-go" to one of the devices if the comparison is between two active systems. If the first four stages (Time Overlap, Line of Sight, Cone Intersection, Friis Tolerance) show overlap, but the frequency requests do not overlap, the broker then considers if outof-band or harmonic interference is a possibility. If out-ofband or harmonic interference is deemed possible, the broker calculates a spatial-spectral mask for the active system transmission(s) that provides frequency and spatial constraints for the transmission. In our experiments, passive systems are given ultimate preference; however, different value assessments can be incorporated to modify the broker if desired.

At the stage of the work presented in this paper, the broker is a mechanism by which cooperative systems can coexist. To deal with non-cooperative interference, interference victims

Fig. 3. Flow diagram showing the broker culling process

would need to sense this interference, report it back to the broker, and request to move to a different frequency. This idea of a "closed-loop broker" could be useful in cases where the broker has control over either the interferer or the interference victim. Additionally, the broker presented in this paper does not consider aggregation of multiple interference sources, which is a logical step in the broker development. This is planned for future work.

A. Stage 1: Time Overlap

In Stage 1 the broker first determines if there is any time overlap within the reported device manifolds. Alg. 1 shows pseudocode for this stage of the broker culling process using the symbols indicated in Table II. All algorithms discussed in this paper reference these same symbols. Based on Line 1, if request A starts before request B and ends after request B begins, time overlap is confirmed. Likewise, line 3 tests if B starts before A and ends after B begins. If neither of these conditions is true, then the two requests do not overlap in time. If no time overlap exists, then the broker exits and does not progress to additional culling stages. If the systems are not using the spectrum at the same time, there can be no interference, regardless of frequency, line of sight, or cone intersection overlap.

Algorithm 1 Stage 1: Temporal Overlap

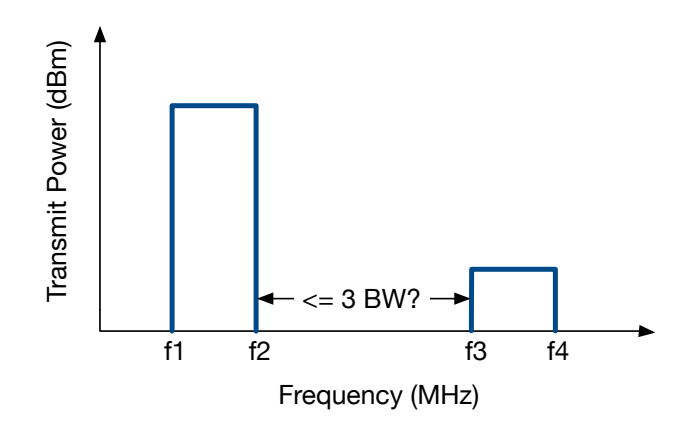
Input: Two user request manifolds (A and B)

Output: Temporal overlap flag

- 1: if $((t_A \le t_B)AND(t_A + \Delta t_A) \ge t_B)$ then
- 2: return TRUE {A starts before B and ends after B begins}
- 3: else if $((t_B \le t_A)AND(t_B + \Delta t_B) \ge t_A)$ then
- 4: **return** TRUE {B starts before A and ends after A begins}
- 5: **else**
- 6: **return** FALSE {A and B do not overlap in time}
- 7: **end if**

B. Stage 2: Frequency Interference Calculation

In Stage 2, the frequency requests of the two systems are first compared for direct overlap. If the requested frequencies overlap, then a no-go must be communicated to one of the systems, or the request of one of the systems must be modified. However, even if no direct overlap is incurred, out-of-band or



4

Fig. 4. Out-of-band interference approximation.

harmonic interference may still be possible. A simple approach was created to account for possible out-of-band interference, as shown in Fig. 4. If the requested transmitters band is within three requested transmitter bandwidths of the receivers requested band, then the potential for out-of-band interference is identified. For example, if the requested transmission band is between f_1 and f_2 , and the receivers requested band is between f_3 and f_4 , then the following situation would indicate the potential for interference:

$$|f_3 - f_2| \le 3|f_2 - f_1| \tag{1}$$

The potential for harmonic interference is identified if a receiver request overlaps the band bounded by twice the frequencies of the requested transmitter band edges:

$$f_4 \ge 2f_1 \tag{2}$$

and

$$f_3 < 2f_2.$$
 (3)

Alg. 2 shows the algorithm for determining if any of these types of frequency interference are present using equations (1) – (3). Line 5 checks for in-band frequency overlap, line 13 checks for out-of-band frequency overlap, and line 15 checks for second harmonic frequency overlap. If interference is deemed possible, a spectral-spatial mask is generated that limits the transmission power at in-band, out-of-band, and/or harmonic frequencies as a function of transmission direction.

Algorithm 2 Stage 2: Frequency Interference

Input: Two user request manifolds (A and B) with temporal overlap, line of sight potential, cone intersection, and receive power tolerance exceeded

Output: Frequency interference flag

```
1: f_{minA} \leftarrow f_A - (BW_A/2)
2: f_{maxA} \leftarrow f_A + (BW_A/2)
3: f_{minB} \leftarrow f_B - (BW_B/2)
4: f_{maxB} \leftarrow f_B + (BW_B/2)
5: if ((f_{min_A} \leq f_{max_B})AND(f_{min_B} \leq f_{max_A})) then
      return TRUE {In-band interference potential}
7: else
      f_1 \leftarrow \min(f_{minA}, f_{minB}) {Lowest low frequency}
8:
      f_2 \leftarrow \min(f_{maxA}, f_{maxB}) {Lowest high frequency}
9:
      f_3 \leftarrow \max(f_{minA}, f_{minB}) {Highest low frequency}
10:
      f_4 \leftarrow \max(f_{maxA}, f_{maxB}) {Highest high frequency}
11:
      if (|f_3 - f_2| \le 3|f_2 - f_1|) then
12:
         return TRUE {Out-of-band interference potential}
13:
      else if ((f_4 \ge 2f_1)AND(f_3 \le 2f_2)) then
14:
15:
         return TRUE {Harmonic interference potential}
      end if
16:
17: end if
18: return FALSE {No frequency interference}
```

C. Stage 3: Friis Calculation

During Stage 3, the power received by each user based on the other users requested transmit power is calculated using the Friis transmission equation:

$$P_r = P_t G_t G_r \left(\frac{\lambda}{4\pi R}\right)^2. \tag{4}$$

Alg. 3 shows the application of (4) with logarithmic units to determine the power received by each user from the other. When the requested transmission power of one device is greater than the provided tolerance of the other device, then the broker determines that there is potential for interference between devices. Following that determination, the broker then proceeds to the next stage of culling. The culling process ends for that pair if the calculated received power by both systems is within its declared receive power tolerance value.

D. Stage 4: Line of Sight

During Stage 4, the broker determines if any users are in line of sight of each other on spherical Earth with a radius matching the equatorial radius on WGS84 Earth reference ellipsoid, as detailed in Alg. 4. The system assumes there is no over-the-horizon propagation, so if the curvature of the Earth prevents line of sight, there will be no interference. This is done by following the method shown in section IV.B of [9]. Line 3 calculates the straight-line distance between the two requests and line 7 calculates the maximum line of sight distance between two users at their given altitudes (a). Line 8 then checks if the distance between the requests is less than or equal to the maximum possible distance. If it is, then the possibility of interference exists, and the culling process continues. Otherwise the user will have no interference.

Algorithm 3 Stage 3: Friis Calculation

Input: Two user request manifolds (A and B) with temporal overlap, line of sight potential, and cone intersection

Output: Power tolerance flag

```
1: c \leftarrow 299792458 {m/s, Speed of light}
2: R \leftarrow euclideanDistance(A, B)
3: P_{RxA} \leftarrow P_{TxB} + G_{TxB} + G_{RxA} + 20 \log_{10}(\frac{c/f_A}{4\pi R})
4: P_{RxB} \leftarrow P_{TxA} + G_{TxA} + G_{RxB} + 20 \log_{10}(\frac{c/f_B}{4\pi R})
```

5: if $(P_{RxA} > T_A)$ then

return TRUE {User A receives more power than the specified receive power tolerance.}

```
7: end if
```

8: **if** $(P_{RxB} > T_B)$ **then**

return TRUE {User B receives more power than the specified receive power tolerance.}

10: **end if**

11: return FALSE {Neither receive power tolerance is exceeded.

Algorithm 4 Stage 4: Line of Sight

Input: Two user request manifolds (A and B) with temporal overlap

Output: Line of sight visible flag

```
1: EARTHRADIUS \leftarrow 6378137 {meters}
```

2:
$$X \leftarrow \sqrt{\sin^2(\frac{\varphi_B - \varphi_A}{2}) + \cos(\varphi_A)\cos(\varphi_B)\sin^2(\frac{\lambda_B - \lambda_A}{2})}$$

3: $D \leftarrow 2 * EARTHRADIUS * X$

4:
$$d_1 \leftarrow \sqrt{a_A * (a_A + 2 * EARTHRADIUS)}$$

5:
$$d_2 \leftarrow \sqrt{a_B * (a_B + 2 * EARTHRADIUS)}$$

6: $d \leftarrow d_1 + d_2$

7:
$$D_{max} \leftarrow d * \frac{2*EARTHRADIUS}{2*EARTHRADIUS + a_A + a_B}$$

8: if $(D \leq D_{max})$ then

return TRUE {The users have the potential to see each other without the curvature of a spherical Earth obstructing them.

return FALSE {The users cannot see each other due to the curvature of a spherical Earth.

12: **end if**

E. Stage 5: Cone Intersection

In Stage 5, a cone intersection calculation is completed that uses the antenna beamwidth reported by the device in its manifold. The calculation in Stage 5 approximates the antenna pattern main beam by using the beamwidth, as shown in Fig. 5. The line of sight and cone intersection algorithms are detailed by Marino and Gasiewski [9], Alg. 5 implements this method. The algorithm checks if the direct vector between the two requests is contained in the cone of each antenna. If both antennas are facing each other, then the culling process will continue. Otherwise there is no possibility of interference, and the process exits.

III. SPATIAL-SPECTRAL MAP DETERMINATION

The Friis transmission equation (4) can be used to generate a spatial-spectral mask limiting the transmitted power consid-

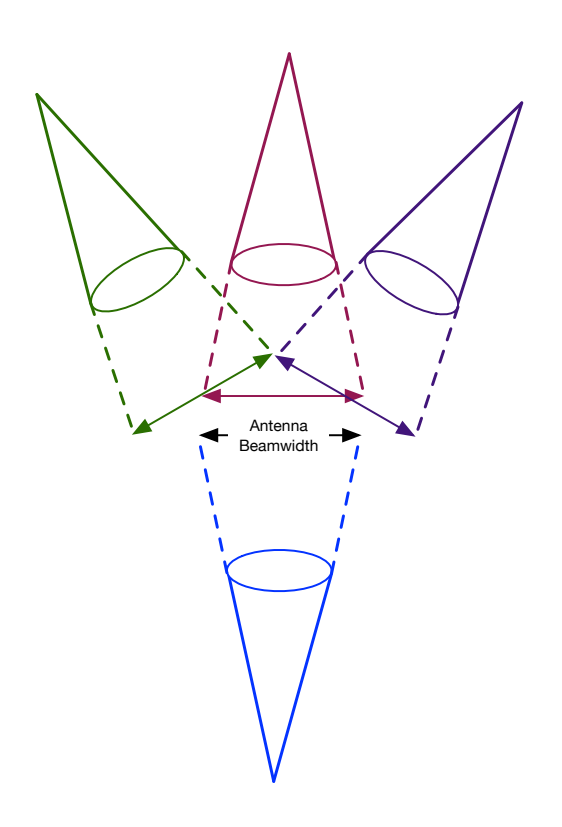


Fig. 5. Broker culling based on beamwidth of the antenna and angular overlap to approximate a device's antenna pattern.

Algorithm 5 Stage 5: Cone Intersection

Input: Two user request manifolds (A and B) with temporal overlap and line of sight potential

Output: Cone intersection flag

- 1: $EARTHRADIUS \leftarrow 6378137$ {meters}
- 2: \vec{R}_A (EARTHRADIUS a_A $[\cos(\varphi_A)\cos(\lambda_A),\cos(\varphi_A)\sin(\lambda_A),\sin(\varphi_A)]$
- 3: \vec{R}_B (EARTHRADIUS a_B $[\cos(\varphi_B)\cos(\lambda_B),\cos(\varphi_B)\sin(\lambda_B),\sin(\varphi_B)]$
- 4: $\vec{R}_{BA} \leftarrow \vec{R}_{B} \vec{R}_{A}$ 5: $\vec{R}_{AB} \leftarrow \vec{R}_{A} \vec{R}_{B}$
- 6: $\vec{P}_A \leftarrow [\cos(\beta_A)\cos(\alpha_A), \cos(\beta_A)\sin(\alpha_A), \sin(\beta_A)]$
- 7: $\vec{P}_B \leftarrow [\cos(\beta_B)\cos(\alpha_B), \cos(\beta_B)\sin(\alpha_B), \sin(\beta_B)]$
- 8: $\gamma_A \leftarrow \arccos(\vec{P}_A \cdot \vec{R}_{BA})/(||\vec{P}_1|| * ||\vec{R}_{BA}||)$
- 9: $\gamma_B \leftarrow \arccos(\vec{P}_B \cdot \vec{R}_{AB})/(||\vec{P}_2|| * ||\vec{R}_{AB}||)$
- 10: $intersect_A \leftarrow FALSE$
- 11: $intersect_B \leftarrow FALSE$
- 12: if $(\gamma_A < .5\theta_A)$ then
- $intersect_A \leftarrow TRUE \{ \text{User A faces User B} \}$ 13:
- 14: end if
- 15: if $(\gamma_B < .5\theta_B)$ then
- $intersect_B \leftarrow TRUE \{ \text{User B faces User A} \}$ 16:
- 18: **return** $(intersect_A)AND(intersect_B)$

Radiometer / 5G Locations - wrt single 5G System (meters)

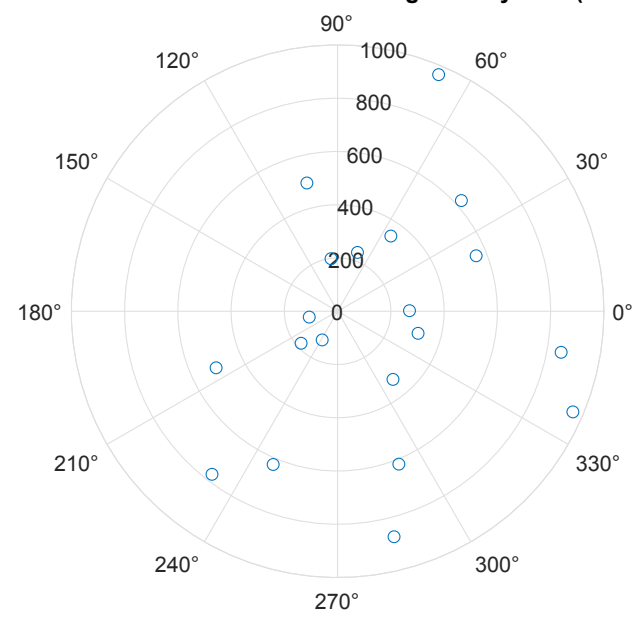


Fig. 6. Simulated spatial transmission scenario for several radiometers with respect to a single 5G system.

ering all devices with known position and interference powers, based on the development by Egbert [30]:

$$P_t(f,\phi) = \min_{0 \le R \le \infty} \left[P_r(f,R,\phi) \frac{(4\pi R)^2}{G_t G_r \lambda^2} \right], \tag{5}$$

where $P_t(f,\phi)$ is the power spectral density in dBm/MHz that can be transmitted at frequency f and the angle ϕ to provide the receiver power spectral density $P_r(f, R, \phi)$, G_t is the transmit antenna power gain in W/W, G_r is the receive antenna power gain in W/W, R is is the radial distance of the receiver, and λ is the wavelength. Equation (5) assumes that the receivers are located at a point and have a negligible angular span with respect to the transmit aperture. The spatialspectral mask consists of the maximum values of P_t , plotted versus f and ϕ .

Fig. 6 shows a simulated spatial transmission scenario for several radiometers with respect to a single 5G system submitted to the broker. Fig. 7 shows an example spatialspectral constraint map for a 5G system and 15 radiometers located within one kilometer. The spatial-spectral constraint map was determined using the spatial, spectral, and calculated Friis tolerances. This constraint map is then passed onto the 5G system or other transmitter and can be used to create a waveform that successfully conforms to these constraints [29], [31]–[34].

IV. EXPERIMENTAL RESULTS

The broker was experimentally tested through trials designed to exercise all five stages of the broker shown in Fig 3. Four specific test cases are presented below. Specific attention is paid to the verification of the spatial-spectral mask generation after Stage 5. Stages 1 and 3 through 5 were extensively tested in Marino and Gasiewski [9]. Thus, all

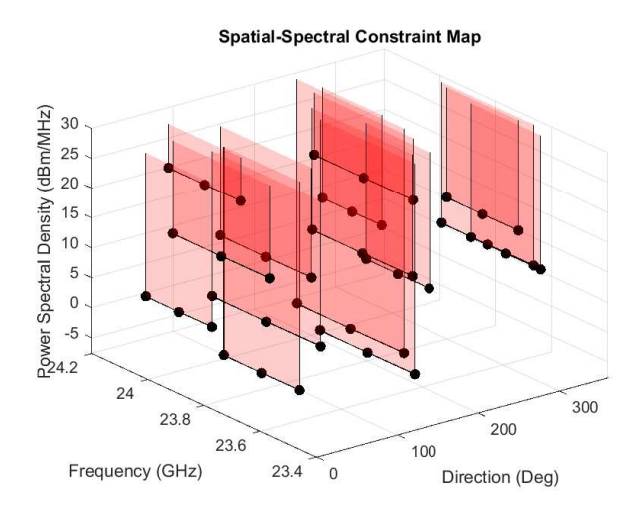


Fig. 7. An example spatial-spectral constraint map for 15 devices that are a mix of radiometers and 5G systems.

of the test cases below meet the criteria needed to advance through all stages, with a focus on how Stage 2 classifies interference. In other words, there is a time overlap in Stage 1, the Friis calculation of Stage 3 indicates potential interference, the devices are within line of sight of each other in Stage 4, and there is a cone intersection in Stage 5. Cases 1 through 4 demonstrate particular examples that are illustrative of the important operating modes of the broker. Each test case demonstrates a 5G device operating in the vicinity of five terrestrial radiometers.

A. Case 1: 5G In-Band Interference to Five Radiometers

Case 1 represents an interference test case for the broker where a 5G device requests an operating bandwidth that directly overlaps the operating bandwidth of the radiometers. The relevant device operation parameters may be found in Table III. The criteria for all stages are met with this test case to indicate the potential of interference and generate a spatialspectral mask. While present allocations require that a 5G device should only be operating at or above 24 GHz and it should never be in-band to a radiometer, this test case is designed to verify that the broker identifies and constructs a spatialspectral mask that is appropriate. The 5G transmitting device requests operation with a center frequency of 23.9 GHz and a bandwidth of 0.40 GHz, an allocation request that is within the operating bandwidths of five nearby radiometers. The radiometers have center frequencies ranging from 23.6 GHz to 23.9 GHz and bandwidths that range from 0.20 GHz to 0.40 GHz with interference levels of -105 dBm to -85 dBm. Fig. 8 shows the calculated spatial-spectral constraint map. When reaching Stage 2 of the culling, the broker properly determines that there is in-band interference to each of the five radiometers and later calculates a constraint map that is based on the radiometer operation parameters. Each shaded region on the plot shown in Fig 8 represents a constraint placed on the 5G operation by a radiometer. This calculated constraint map is then passed onto the 5G system to provide limits to

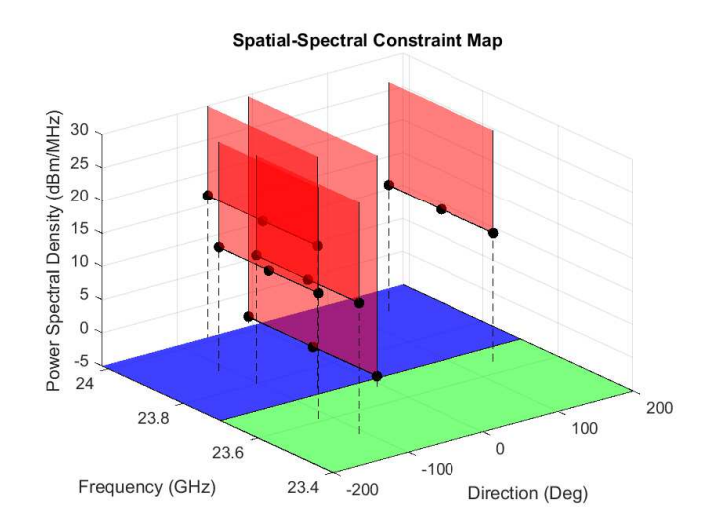


Fig. 8. Case 1: Spatial-Spectral Constraint Map when a single 5G device operating at 23.9 GHz interferes with five radiometers operating in a frequency range from 23.6 GHz to 23.9 GHz. The blue region represents frequencies in-band and the green region represents frequencies out-of-band to the 5G device.

the 5G transmission at these combinations of frequency and direction.

TABLE III

CASE 1: 5G AND RADIOMETER DEVICE PARAMETERS, IN-BAND
INTERFERENCE TO FIVE RADIOMETERS

	5G System	Radiometer Ranges
Center Frequency	23.9 GHz	23.6 GHz – 23.9 GHz
Bandwidth	0.40 GHz	0.20 GHz – 0.40 GHz
Interference Levels	N/A	-105 dBm85 dBm

B. Case 2: 5G Potential Out-of-Band Interference to Five Radiometers

Case 2 represents a scenario where a 5G device has the potential for out-of-band interference to five radiometers. This potential for out-of-band interference is identified by calculating according to the simple algorithm presented in Section II-B and equation (1). As in Case 1, all criteria are met in each other stage(i.e. time overlap, Friis tolerance, line of sight, and cone intersection) to be dependent on Stage 2 (i.e. frequency interference calculations). Here the 5G device is requesting an operating center frequency of 24.5 GHz, which is within three bandwidths of the operating frequency of the five radiometers as described in equation (1). The 5G device has an operating bandwidth of 0.40 GHz and the radiometers have operating bandwidths that range from 0.20 GHz to 0.40 GHz having interference levels that range from -105 dBm to -85 dBm as shown in Table IV. Using equation (1), the broker correctly identifies that the 5G device would interfere with all five radiometers and calculates a spatial-spectral constraint map, shown in Fig 9. This spatial-spectral constraint map is then passed onto the 5G system to incorporate those constraints into the transmitted wave pattern to avoid interference with the identified five local radiometers.

TABLE IV
CASE 2: 5G AND RADIOMETER DEVICE PARAMETERS, POTENTIAL
OUT-OF-BAND INTERFERENCE TO FIVE RADIOMETERS

	5G System	Radiometer Ranges
Center Frequency	24.5 GHz	23.6 GHz – 23.9 GHz
Bandwidth	0.40 GHz	0.20 GHz – 0.40 GHz
Interference Levels	N/A	-105 dBm – -85 dBm

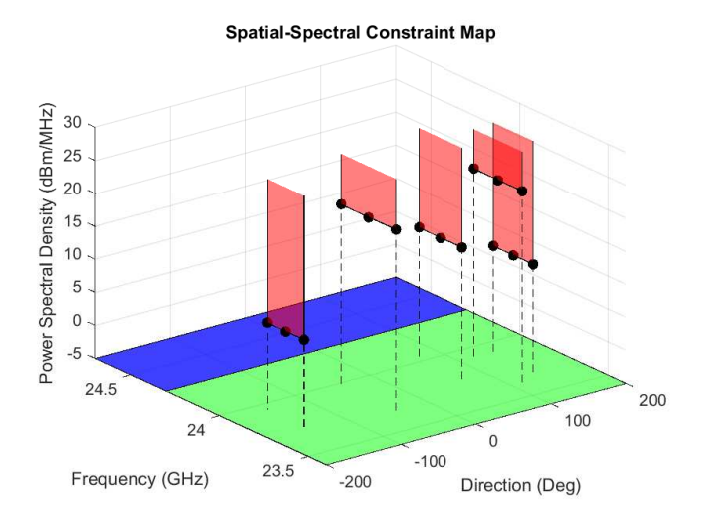


Fig. 9. Case 2: Spatial-spectral constraint map when a single 5G device operating at 24.5 GHz with a 0.40 GHz bandwidth interferes with five radiometers operating in a frequency range from 23.3 GHz to 23.9 GHz (all within 3 bandwidths). The blue region represents frequencies in-band and the green region represents frequencies out-of-band to the 5G device.

C. Case 3: 5G Harmonic Interference to Five Radiometers

Case 3 demonstrates the handling of potential harmonic interference to five radiometers. As with Cases 1 and 2, all criteria are met in Stages 1, 3, 4, and 5 indicating that there is operation within the same time period (time overlap), within range as calculated by the Friis equation, line of sight between devices, and cone intersection (the antennas have intersection). Section II-B discusses calculating the potential for harmonic interference and presents these calculations in equations (2) and (3). As shown in Table V, the 5G device has a center frequency of 26 GHz and a bandwidth of 0.4 GHz. The 5G device operates in the vicinity of five radiometers with center frequencies ranging from 50 GHz to 58 GHz, bandwidths from 0.27 GHz to 0.40 GHz, and interference threshold levels that span -105 dBm to -85 dBm. Using equations (2) and (3), the broker identifies that the 5G device has the potential for harmonic interference with the radiometers operating with center frequencies of 50 GHz to 58 GHz. The resulting spatialspectral constraint map is shown in Fig 10.

TABLE V
CASE 3: 5G AND RADIOMETER DEVICE PARAMETERS, POTENTIAL
HARMONIC INTERFERENCE TO FIVE RADIOMETERS

	5G System	Radiometer Ranges
Center Frequency	26 GHz	50 GHz – 58 GHz
Bandwidth	0.40 GHz	0.27 GHz – 0.40 GHz
Interference Levels	N/A	-105 dBm85 dBm

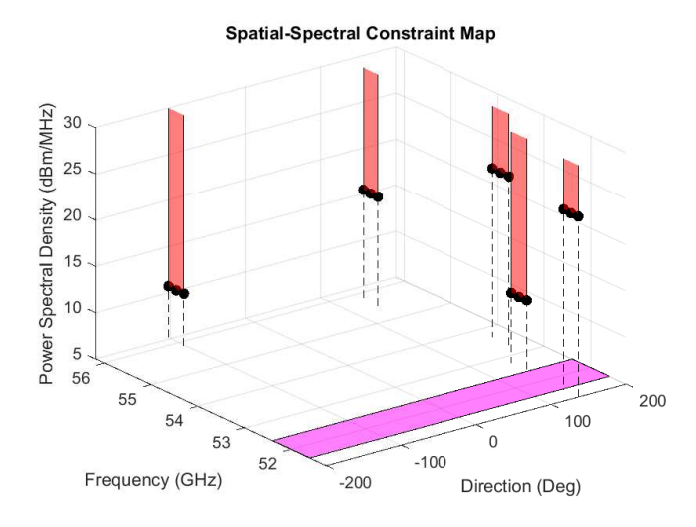


Fig. 10. Case 3: Spatial-spectral constraint map when a single 5G device operating at 26 GHz with a 0.40 GHz bandwidth could harmonically interfere with five radiometers operating in a frequency range from 50 GHz to 58 GHz due to harmonics. The magenta region represents frequencies in the second harmonic of the 5G device.

D. Case 4: No Interference

Case 4 is the final case when there is no interference between a 5G system and five radiometers to verify the operation of the broker presented in this paper. Once more, the criteria of culling Stages 1, 3, 4, and 5 are met, indicating that the 5G and the five radiometer devices are operating within the same time period, within the line of sight based upon antenna and power-level assumptions. However, for this case, there is no potential for either in-band or out-of-band interference, so the consideration of potential interference is dismissed from the culling process after Stage 2 (frequency overlap). Table VI presents the device operating parameters for this coexistence scenario. The 5G transmitter operates at 26 GHz with a bandwidth of 0.4 GHz. The five radiometers operate with center frequencies of 23.4 GHz to 23.9 GHz, having bandwidths that range from 0.27 GHz to 0.40 GHz. The broker correctly identifies that the 5G device will not interfere with five radiometers and flags the 5G system for unencumbered operation.

TABLE VI
CASE 4: NO IN-BAND OR OUT-OF-BAND INTERFERENCE FROM A 5G
SYSTEM TO FIVE RADIOMETERS

	5G System	Radiometer Ranges
Center Frequency	26 GHz	23.4 GHz – 23.9 GHz
Bandwidth	0.40 GHz	0.27 GHz – 0.40 GHz
Interference Levels	N/A	-105 dBm85 dBm

V. CONCLUSIONS

A dynamic spatial-spectral broker that protects passive systems from both in-band and out-of-band interference from nearby active transmitters has been presented. In potential out-of-band or harmonic interference scenarios, the broker generates a spatial-spectral mask to limit the active device

transmitter, preventing potential interference. In-band, outof-band, and harmonic interference can be avoided by limiting active device transmissions using this spatial-spectral masking method. This method will allow basic brokers to be deployed that can protect the use of active transmissions near, or harmonically related to, bands that are used for passive receivers. Additionally, this method is capable of allowing passive receivers to opportunistically use additional bands other than their original assigned bands. Significant spectrum-use flexibility and adaptivity will be provided by the implementation of this method in practice.

ACKNOWLEDGMENTS

This research was funded by the National Science Foundation (Grant No. 2030243). The authors are grateful to Kayla Sanders for assistance in the development and testing of the initial broker code.

REFERENCES

- [1] D. Lubar, D. Kunkee, and L. Cahsin, "Developing a Sustainable Spectrum Approach to Deliver 5G Services and Critical Weather Forecasts," in *Center for Space Policy and Strategy, The Aerospace Corporation*, 2020.
- [2] E. Niiler, 5g networks could throw weather forecasting into chaos, 2019. [Online]. Available: https://www.wired.com/story/5g-networks-could-throw-weather-forecasting-into-chaos/.
- [3] E. Johnson and F. Lucas, Letter to Hon. Gene L. Dodaro, United States House of Representatives, Committee on Science, Space, and Technology, 2019.
- [4] H. Kour, R. K. Jha, and S. Jain, "A comprehensive survey on spectrum sharing: Architecture, energy efficiency and security issues," *Journal of Network and Computer Applications*, vol. 103, pp. 29–57, 2018, ISSN: 1084-8045. DOI: 10.1016/j.jnca.2017.11.010.
- [5] D. Tarek, A. Benslimane, M. Darwish, and A. M. Kotb, "Survey on spectrum sharing/allocation for cognitive radio networks internet of things," *Egyptian Informatics Journal*, vol. 21, no. 4, pp. 231–239, 2020, ISSN: 1110-8665. DOI: 10.1016/j.eij.2020.02.003.
- [6] L. Kulacz, P. Kryszkiewicz, and A. Kliks, "Waveform flexibility for network slicing," *Wireless Communications and Mobile Computing*, vol. 2019, pp. 1–15, 2019, ISSN: 1530-8669. DOI: 10.1155/2019/6250804. [Online]. Available: https://browzine.com/articles/291729177.
- [7] R. H. Tehrani, S. Vahid, D. Triantafyllopoulou, H. Lee, and K. Moessner, "Licensed spectrum sharing schemes for mobile operators: A survey and outlook," *IEEE Communications Surveys Tutorials*, vol. 18, no. 4, pp. 2591–2623, 2016. DOI: 10.1109/COMST.2016. 2583499.
- [8] J. Chong, "Manifold-based system for passive-active spectrum sharing," in *M.S. Thesis, University of Colorado at Boulder*, accepted May 2014.

- [9] J. Marino and A. J. Gasiewski, "A broker based scheme for spectrum sharing," in 2017 IEEE International Geoscience and Remote Sensing Symposium (IGARSS), 2017, pp. 3455–3458. DOI: 10.1109/IGARSS.2017.8127742.
- [10] M. Hyhty, A. Mmmel, X. Chen, A. Hulkkonen, J. Janhunen, J.-C. Dunat, and J. Gardey, "Database-assisted spectrum sharing in satellite communications: A survey," *IEEE Access*, vol. 5, pp. 25322–25341, 2017. DOI: 10.1109/ACCESS.2017.2771300.
- [11] Y. Luo, L. Gao, and J. Huang, "Spectrum broker by geolocation database," in 2012 IEEE Global Communications Conference (GLOBECOM), 2012, pp. 5427–5432. DOI: 10.1109/GLOCOM.2012.6503984.
- [12] M. D. Zulfiqar, S. Roy, and S. Mishra, "Dynamic spectrum access network scaling with multiple users: A market-based analysis," in 2019 IEEE International Symposium on Dynamic Spectrum Access Networks (DySPAN), 2019, pp. 1–8. DOI: 10.1109/DySPAN.2019. 8935788.
- [13] Order on Reconsideration and Second Report and Order in the Matter of Amendment of the Commissions Rules with Regard to Commercial Operations in the 3550-3650 MHz Band, FCC 16-55, Federal Communications Commission, 2016.
- [14] Report and Order and Further Notice of Proposed Rulemaking In the Matter of Unlicensed Use of the 6 GHz Band Expanding Flexible Use in Mid-Band Spectrum Between 3.7 and 24 GHz, FCC 20-51, Federal Communications Commission, 2020.
- [15] M. Koziol, "What is wi-fi 7? great capacity, less latencyhere's how ieee 802.11be achieves both," *IEEE Spectrum*, 2022.
- [16] L. Yin, S. Li, H. Zhu, Y. Ma, Y. Teng, and H. Liu, "Reduced-power almost black subframe based pulse radar spectrum sharing for lte system," *IEEE Transac*tions on Electromagnetic Compatibility, vol. 60, no. 5, pp. 1223–1230, 2018. DOI: 10.1109/TEMC.2018. 2810250.
- [17] A. F. Martone, "Cognitive radar demystified," *URSI Radio Science Bulletin*, vol. 2014, no. 350, pp. 10–22, 2014. DOI: 10.23919/URSIRSB.2014.7910111.
- [18] S. Haykin, "Cognitive radar: A way of the future," *IEEE Signal Processing Magazine*, vol. 23, no. 1, pp. 30–40, 2006. DOI: 10.1109/MSP.2006.1593335.
- [19] H. Griffiths, L. Cohen, S. Watts, E. Mokole, C. Baker, M. Wicks, and S. Blunt, "Radar spectrum engineering and management: Technical and regulatory issues," *Proceedings of the IEEE*, vol. 103, no. 1, pp. 85–102, 2015. DOI: 10.1109/JPROC.2014.2365517.
- [20] B. H. Kirk, R. M. Narayanan, K. A. Gallagher, A. F. Martone, and K. D. Sherbondy, "Avoidance of time-varying radio frequency interference with software-defined cognitive radar," *IEEE Transactions* on Aerospace and Electronic Systems, vol. 55, no. 3, pp. 1090–1107, 2019. DOI: 10.1109/TAES.2018. 2886614.

- [21] B. H. Kirk, M. A. Kozy, K. A. Gallagher, R. M. Narayanan, R. M. Buehrer, A. F. Martone, and K. D. Sherbondy, "Cognitive software-defined radar: Evaluation of target detection with rfi avoidance," in 2019 IEEE Radar Conference (RadarConf), 2019, pp. 1–6. DOI: 10.1109/RADAR.2019.8835498.
- [22] B. H. Kirk, A. F. Martone, K. D. Sherbondy, and R. M. Narayanan, "Performance analysis of pulse-agile sdradar with hardware accelerated processing," in 2020 IEEE International Radar Conference (RADAR), 2020, pp. 117–122. DOI: 10.1109/RADAR42522.2020.9114561.
- [23] E. Selvi, R. M. Buehrer, A. Martone, and K. Sherbondy, "On the use of markov decision processes in cognitive radar: An application to target tracking," in 2018 IEEE Radar Conference (RadarConf18), 2018, pp. 0537–0542. DOI: 10.1109/RADAR.2018.8378616.
- [24] T. Schipper, S. Prophet, M. Harter, L. Zwirello, and T. Zwick, "Simulative prediction of the interference potential between radars in common road scenarios," *IEEE Transactions on Electromagnetic Compatibility*, vol. 57, no. 3, pp. 322–328, 2015. DOI: 10.1109/TEMC. 2014.2384996.
- [25] G. M. Brooker, "Mutual interference of millimeter-wave radar systems," *IEEE Transactions on Electromagnetic Compatibility*, vol. 49, no. 1, pp. 170–181, 2007. DOI: 10.1109/TEMC.2006.890223.
- [26] J. Sevic, R. Baeten, G. Simpson, and M. Steer, "Automated large- signal load-pull characterization of adjacent-channel power ratio for digital wireless communication systems," in 46th ARFTG Conference Digest, 1995, pp. 64–70. DOI: 10.1109/ARFTG.1995. 327134.
- [27] C. Latham, A. Egbert, C. Baylis, L. Cohen, and R. J. Marks, "Joint radar amplifier circuit and waveform optimization for ambiguity function, power-added efficiency, and spectral compliance," *IEEE Transactions on Aerospace and Electronic Systems*, vol. 55, no. 3, pp. 1190–1199, 2019. DOI: 10.1109/TAES.2019.2909725.
- [28] R. Fano, "Theoretical limitations on the broad-band matching of arbitrary impedances," *Journal of the Franklin Institute*, vol. 249, pp. 139–154, 1950.
- [29] J. Roessler, A. Goad, A. Egbert, C. Baylis, A. Martone, R. J. Marks, and B. Kirk, "Enhancing frequency-agile radar range over a broad operating bandwidth with reconfigurable transmitter amplifier matching networks," in 2021 IEEE Radar Conference (RadarConf21), 2021, pp. 1–5. DOI: 10.1109 / RadarConf2147009.2021. 9455307.
- [30] A. Egbert, C. Latham, C. Baylis, and R. J. Marks, "Multi-dimensional coexistence: Using a spatialspectral mask for spectrum sharing in directional radar and communication," in 2018 Texas Symposium on Wireless and Microwave Circuits and Systems (WMCS), 2018, pp. 1–6. DOI: 10.1109/WMCaS.2018.8400641.
- [31] C. Baylis, A. Egbert, J. Alcala-Medel, A. Dockendorf, A. Martone, and R. J. Marks, "Real-time circuit recon-

- figuration for a cognitive software-defined radar transmission: A new paradigm in spectrum sharing," in 2019 IEEE International Symposium on Electromagnetic Compatibility, Signal Power Integrity (EMC+SIPI), 2019, pp. 448–450. DOI: 10.1109/ISEMC.2019.8825209.
- [32] C. Calabrese, A. Dockendorf, A. Egbert, B. Herrera, C. Baylis, and R. J. Marks, "Fast switched-stub impedance tuner reconfiguration for frequency and beam agile radar and electronic warfare applications," in 2020 IEEE International Radar Conference (RADAR), 2020, pp. 94–98. DOI: 10.1109/RADAR42522.2020.9114834.
- [33] C. Calabrese, J. Roessler, A. Egbert, A. Fisher, C. Baylis, Z. V. Missen, M. A. Khater, D. Peroulis, and R. J. Marks, "A plasma-switch impedance tuner for real-time, frequency-agile, high-power radar transmitter reconfiguration," in 2021 IEEE MTT-S International Microwave Symposium (IMS), 2021, pp. 585–588. DOI: 10.1109/IMS19712.2021.9574975.
- [34] A. Egbert, K. Gallagher, B. Kirk, M. Kozy, A. Martone, C. Baylis, E. Viveiros, and R. J. Marks, "The effect of real-time radar transmitter amplifier impedance tuning on range and doppler detection accuracy," in 2019 IEEE Texas Symposium on Wireless and Microwave Circuits and Systems (WMCS), 2019, pp. 1–4. DOI: 10.1109/ WMCaS.2019.8732549.



Adam C. Goad (Graduate Student Member, IEEE) received the B.S. degree in electrical and computer engineering from Baylor University, Waco, TX, USA, in 2019.

He is currently working towards the M.S. and Ph.D. degrees in electrical and computer engineering at Baylor University. His research interests include spectral coexistence techniques and real-time circuit optimization, especially for array-based joint radar communication and 5G systems.



Sarah A. Seguin (S'99, M'09, SM'15) is a senior project engineer at The Aerospace Corporation. She was formerly the Executive Vice President of Operations and still remains a co-owner of Third Iron, a software development company focused on academic research information systems. She has worked as a researcher and faculty-in-resident at a number of notable institutions such as Baylor University, the Naval Research Laboratory, the University of Kansas, Apple Computer, and Boston Scientific. She received her B.S., MS., and Ph.D. in Electrical

Engineering from the Missouri University of Science and Technology. She is currently the chair of the Spectrum Engineering Technical Committee 6 (TC6) of the IEEE Electromagnetic Compatibility (EMC) Society. Her research areas include spectrum engineering, Electromagnetic Compatibility, Antenna Design, Electromagnetic Modeling, Radar, and Electromagnetics.



Charles Baylis (Senior Member, IEEE) received the B.S., M.S., and Ph.D. degrees in electrical engineering from the University of South Florida, Tampa, FL, USA, in 2002, 2004, and 2007, respectively.

He is a Professor of Electrical and Computer Engineering and Director of the Wireless and Microwave Circuits and Systems Program at Baylor University, where he has served since 2008. Dr. Baylis serves as Director of SMART Hub (Hub for Spectrum Management with Adaptive and Reconfigurable Technology), a United States Department of

Defense Spectrum Innovation Center commissioned in 2023, headquartered at Baylor, and involving 29 researchers from 17 universities. His research interests include reconfigurable wireless circuits and systems for spectral coexistence.

Dr. Baylis founded the annual Texas Symposium on Wireless and Microwave Circuits and Systems, where he serves as the Chair for the Executive Committee



Trevor Van Hoosier (Graduate Student Member, IEEE) received the B.S. degree in electrical and computer engineering from Baylor University, Waco, TX, USA, in 2021.

He is currently working toward the M.S. degree in electrical and computer engineering at Baylor University. His research interests include spectral coexistence techniques and real-time circuit optimization for application to radar transmit amplifiers and 5G systems.



Emma Lever (Graduate Student Member, IEEE) received the B.S. degree in Electrical and Computer Engineering from Baylor University, Waco, TX, USA, in 2023.

She is currently working toward the Ph.D. degree in Electrical and Computer Engineering at Baylor University. Her research includes spectral coexistence circuitry as well as its impact on signal processing techniques.



Albin J. Gasiewski (StM'81, M'88, SM'95, F'02) is Professor of Electrical and Computer Engineering at the University of Colorado at Boulder and Director of the CU Center for Environmental Technology (CET). He received the Ph.D. degree in electrical engineering and computer science from the Massachusetts Institute of Technology in 1989. Previously, he received the M.S. and B.S. degrees in electrical engineering and the B.S. degree in mathematics from Case Western Reserve University in 1983. From 1989 to 1997 he was a faculty member

at the Georgia Institute of Technology, in Atlanta GA. From 1997 through 2005 he worked for the U.S. National Oceanic and Atmospheric Administration's (NOAA) Environmental Technology Laboratory in Boulder, Colorado, USA, where he became Chief of ETLs Microwave Systems Development Division. He has developed and taught graduate courses on electromagnetics, antennas, remote sensing, instrumentation, and wave propagation theory. Prof. Gasiewski is a Co-Founder and Chief Scientist of Orbital Micro Systems, Inc.

Prof. Gasiewski is a Fellow of the IEEE, Past President (2004-2005) of the IEEE Geoscience and Remote Sensing Society, and founding member of the IEEE Committee on Earth Observation (ICEO). He is a member of the American Meteorological Society, the American Geophysical Union, the International Union of Radio Scientists (URSI), Tau Beta Pi, and Sigma Xi. From 2009-2011 he served as Chair of USNC/URSI Commission F. He served on the U.S. National Research Council's Committee on Radio Frequencies (CORF) from 1989-1995. He was the General Co-chair of IGARSS 2006, in Denver, Colorado, and a recipient of the 2006 Outstanding Service Award and the 2017 Education Award from the GRSS.



Aravind Venkitasubramony (Graduate Student Member, IEEE) received the B.Tech. degree in electronics and communication engineering from the University of Kerala, Thiruvananthapuram, India, in 2006, and the M.Eng. degree in space engineering from the University of Michigan, Ann Arbor, MI, USA, in 2013. He is pursuing the Ph.D. degree in electrical engineering with the Center for Environmental Technology (CET), University of Colorado Boulder, Boulder, CO, USA., He has worked as a Spacecraft Operations Engineer with the ISRO

Telemetry Tracking and Command Network (ISTRAC), Bengaluru, India, from 2007 to 2015. His research interests include microwave radiometry, RFI detection and mitigation techniques, RF instrumentation and systems engineering.



Robert J. Marks II (Life Fellow, IEEE) is a Distinguished Professor of Electrical and Computer Engineering at Baylor University, Waco, TX, USA, and a Senior Fellow and Director of the Walter Bradley Center for Natural & Artificial Intelligence, Seattle, WA, USA. Marks is author of the book Non-Computable You: What You Do That Artificial Intelligence Never Will (Discovery Institute, 2022). He is co-author of the books For a Greater Purpose: The Life and Legacy of Walter Bradley (Erasmus Press, 2020), Neural Smithing: Supervised Learning

in Feedforward Artificial Neural Networks (The MIT Press, 1999) and Introduction to Evolutionary Informatics (World Scientific, 2017).

Dr. Marks, II, is a Fellow of Optica (formerly the Optical Society of America). He is the Editor-in-Chief of BIO-Complexity and the former Editor-in-Chief of the IEEE TRANSACTIONS ON NEURAL NETWORKS AND LEARNING SYSTEMS. His professional awards include the NASA Tech Brief Award and the IJCNN Pioneer in Neural Network Award. He is the Faculty Advisor for the Ratio Christi and American Scientific Affiliation Student Chapters at Baylor University. He has a Bacon-Erds number of five.